

Impact Testing of 3D Printed Kevlar-Reinforced Onyx Material

Mackenzie Scrocco¹, Timothy Chamberlain¹, Chloe Chow¹, Logan Weinreber¹, Edward Ellks¹,
Connor Halford², Pedro Cortes¹, Brett P. Conner¹

¹Youngstown State University

²Youngstown Business Incubator

Abstract:

Kevlar is a common reinforcement used in composites for applications requiring impact resistance. This research evaluated the impact performance of 3D printed continuously reinforced Kevlar fiber on 3D printed nylon composites containing chopped carbon fiber (CCF). The 3D printer used was a Markforged Mark Two material extrusion system, and Onyx is the trade name of Markforged's nylon/CCF material. In this work, a diverse number of composite architecture designs including type of infill pattern, number of Kevlar layers, and location of Kevlar layers were investigated. The printed specimens were characterized using a Charpy impact testing and gas gun ballistic testing. Results were compared on the basis of weight and estimated part cost.

Keywords: impact testing, kevlar, Markforged, projectile

1. Introduction

The impact resistance of materials is needed for a variety of applications. In aviation, gas turbine engine containment rings prevent detached rotating components from exiting the engine nacelle and impacting the aircraft [1]. Forward aircraft structures and cockpit windows need to resist bird strike and hail impact [2–4]. Manned space vehicles require a level of protection against micrometeoroid impact [5]. Similarly, high performance materials are desired for body and vehicle armor to stop projectiles while minimizing weight [6,7].

Additive manufacturing (AM) provides advantages over conventional manufacturing processes by providing a more capable and cost effective means to produce complex geometries yielding more functional designs, and an efficient means of customization [8]. Indeed, AM allows for mass customization, production on demand or production at the point of need, and quantity flexibility leading to affordable low volume production and the ability to shift into

higher production quantities on the same equipment . These advantages can be brought into the design and fabrication of impact resistant structures. A key first step is understanding the mechanical performance of these 3D printed structures.

Often the optimal combination of impact resistance and weight come from multi-material solutions [9–11]. Therefore, multi-material additive manufacturing solutions should be of interest to create lightweight-high performance systems. One approach is to provide fiber reinforcement to polymeric parts. The Markforged Mark Two shown in Figure 1 is a desktop material extrusion 3D printer. The Mark Two is capable of printing a filament consisting of nylon and chopped carbon fiber (CCF). This material is called Onyx and is 1.4 times stronger and stiffer than ABS [12]. The Mark Two also has a second extruder which allows for a continuous fiber reinforcement within the printed part. The Mark Two is capable of printing the following materials as fiber reinforcement: Carbon Fiber, Fiberglass, Kevlar. Markforged claims the Mark Two has a 10 micron accuracy meaning that a build could be paused, the build plate removed, and objects such as threaded nuts or bolts could be incorporated into the printed parts and the build plate brought back into the build envelope for continued printing. This feature was not verified in this study.

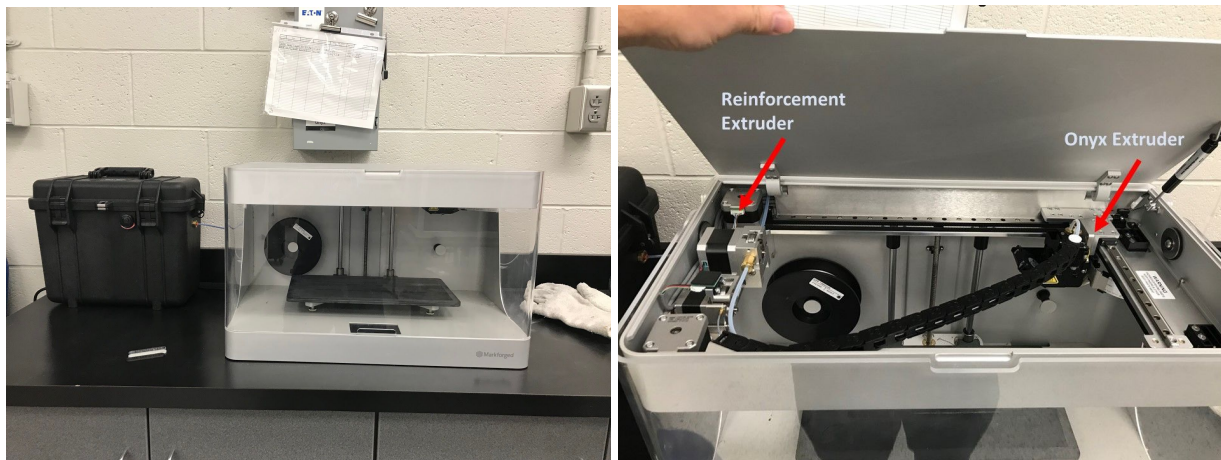


Figure 1: The Markforged Mark Two printer is shown at left. At right the two extruder nozzles are shown. The left nozzle in the image is for the continuous fiber reinforcement and the fiber filament spool is visible. The Onyx nozzle is at the right of the image.

The Markforged Eiger software is used for build processing including file slicing, layer heights, infill pattern selection, reinforcement pattern selection, location of reinforcement, and location of parts on the build plate. The Onyx layer heights that can be selected for unreinforced parts are: 0.100, 0.125, and 0.200 mm. As shown in Figure 2, several Onyx infill patterns can be selected: triangular (TRI), rectangular (RECT), and hexagonal (HEX). There are also options for reinforcement infill patterns as shown in Figure 3. The first reinforcement pattern is isotropic

(ISO) which is similar to the RECT infill pattern. The second fiber reinforcement pattern is concentric (CON), which prints concentric rings of fiber around the perimeter of the part. ISO and CON can be combined in the same layer. If reinforcement is selected, the Onyx layer height is restricted to only 0.100 mm. Combinations of these parameters can be used to create composite structure architectures.

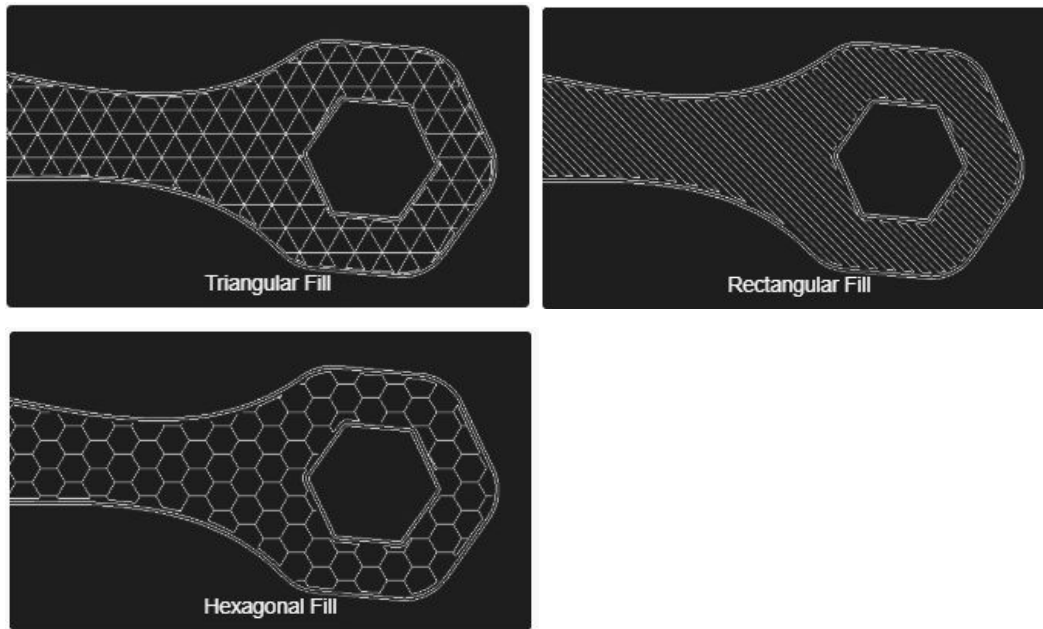


Figure 2: Onyx infill patterns

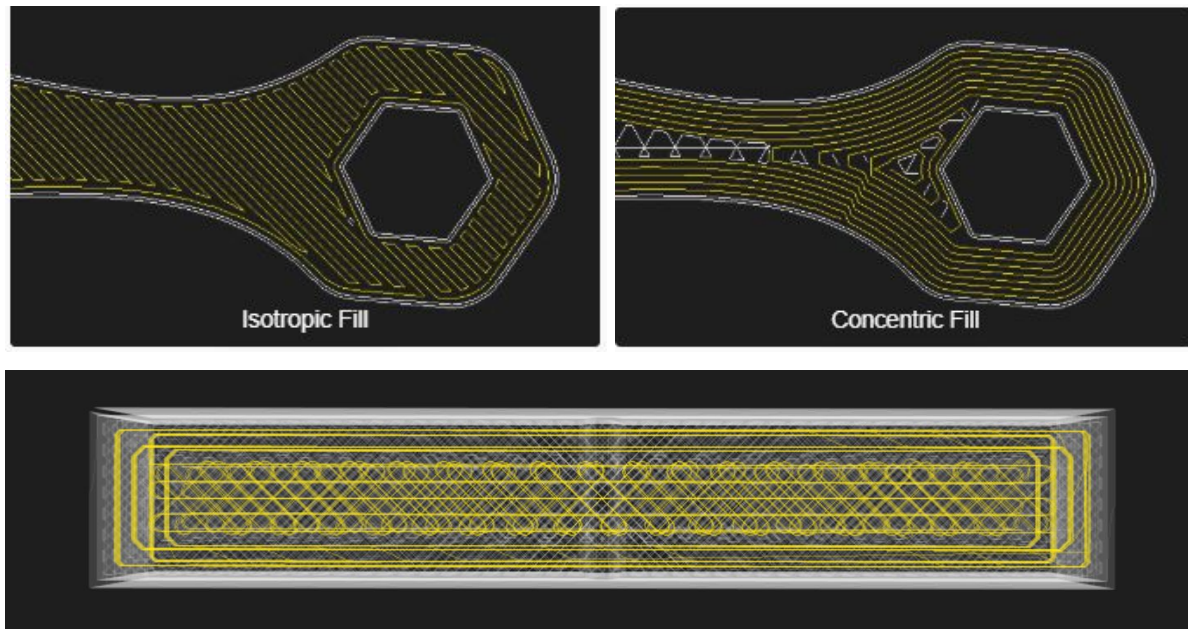


Figure 3: Continuous fiber reinforcement fill patterns. Top: isotropic, concentric. Bottom: Charpy v-notch specimen with combined isotropic and concentric reinforcement.

The effect on tensile properties of continuous fiber reinforcement of 3D printed parts was evaluated by Melenka, et al [13]. In their study, the researchers used a Markforged Mark One printer. The base material was nylon not Onyx, and the continuous reinforcement material selected was Kevlar. The continuous fiber fill parameter was chosen, and specimens with zero reinforcement rings (0% volume fraction), two rings (4.04% volume fraction), four rings (8.08% volume fraction), and five rings (10.1% volume fraction) were evaluated. The researchers found that the tensile modulus of the nylon was on the order of 1 MPa and the ultimate tensile strength was less than 10 MPa. The researchers experimentally determined that the Kevlar reinforcement resulted in dramatic increases in the elastic moduli and the tensile strength. For the two rings, the modulus was 1767.2 MPa and the strength was near 30 MPa. In contrast, for the four rings, the modulus was 6920.0 MPa with a strength near 60 MPa; whereas for the five rings, the modulus was 9001.2 MPa and the measured strength was near 90 MPa.

Camirero et al examined the effect of carbon fiber, Kevlar, and glass fiber reinforcement on nylon (not Onyx) using 3D printed Charpy v-notch specimens manufactured on a Markforged Mark Two printer [14]. The architecture chosen involved a rectangular fill of maximum density with isotropic reinforcement. Three process parameters were examined: layer thickness of unreinforced samples, build orientation, and fiber content. The researchers printed Charpy specimens following the ASTM D6110 specification, and these were printed in two orientations. The first was called the “Flat” direction where the specimen lies flat on the XY plane of the build plate and the notch in the X direction (implying a fracture propagation in the X orientation with the notch thickness being in the Z direction). The second orientation was referred to as the “On-edge” direction where the notch faced in the Z direction and therefore fracture propagated in the Z-direction. They concluded that impact strength increased as layer thickness increased for the flat orientation. However, impact strength decreased in the on-edge direction. By printing flat and on-edge specimens with reinforcement layers being oriented in the XY plane of the build, the researchers evaluated the effects of orientation and reinforcement. On-edge samples exhibited higher impact strengths than flat samples. Impact strength was also shown to have increased with fiber volume content. Finally, glass fiber showed the best impact performance followed by Kevlar and lastly the carbon fiber reinforcement [14].

2. Methodology

In this work, the Onyx without reinforcement, and the Kevlar reinforced Onyx composite were 3D printed and then mechanically evaluated under dynamic impact conditions. Here, two forms of testing were used to characterize architectures. The first was a Charpy v-notch impact testing, and the second a gas gun projectile testing.

The Charpy v-notch testing was carried out in order to screen composite architectures for impact resistance, since Charpy specimens are inexpensive as compared to the gas gun targets. Energy absorbed, cost, and weight were the evaluation criteria for this testing. It is worth mentioning, that the Charpy v-notch testing equipment at YSU is for metals testing (ASTM E23). As a result, the Charpy v-notch specimen geometry from ASTM E23 was used. The specimen dimensions were 10 mm x 10 mm x 55 mm with the notch edges each being 2 mm long at a 45 degree angle from each other with a fillet radius of 0.25 mm. If absolute values were of interest instead of comparative, ASTM D6110 – 18 would be more suitable. Twenty architectures were designed for the Charpy testing. The architectures are defined in Table 1. Layer thickness, Onyx infill, and Kevlar reinforcement parameters were here investigated.

Specimen orientations are shown in Figure 4. “XY Notch Down” Charpy specimens had the length and width in the XY build plane but the notch was face down. “XY Notch Side” Charpy specimens had the length and width in the XY build plane but the notch was oriented in the side direction. Z oriented specimens had the length parallel to the Z axis. For comparison, XY Notch Down corresponds to the on-edge orientation from [14], while XY Notch Side corresponds to flat. All reinforcements were printed in the XY plane.

The YSU Gas Gun Launcher, by REL Inc., shown in Figure 5 is used to accelerate projectiles at chosen pressures for testing the impact strength of materials. Projectiles are held by a plastic sabot. The cylindrical sabot is placed in a pressured chamber, which release the projectile through a pressure differential created by opening a release valve. Once the projectile is fired, it travels through piping until it hits the target securely mounted in a trunk-frame. The gas-gun contains a chronograph that measures the projectile velocity. Here, the impact energy is evaluated by using the kinetic energy. For this gas gun testing, McMaster Carr hardened 440 stainless steel spherical bearings were used as the projectiles. These bearings have an 8 mm diameter and were measured to have an average mass of 2.0550 g. The projectile diameter was greater than the thickness of the plates (101 mm x 101 mm x 6 mm). For most tests, a 100 psi pressure was selected which normally corresponds to a velocity of on the order of 250 m/s. The sabots consisted of 3D printed ABS plastic, manufactured on Lulzbot TAZ 6 and CreatorBot3D desktop printers. The sabots were 25 mm in diameter and 25.5 mm tall, and contained an 8mm center hole, where the steel bearing was placed. It is worth mentioning that the targets used in gas gun projectile testing needed considerably more material than the Charpy specimens, and therefore, were relatively expensive.

Both Charpy and gas gun specimens were optically characterized using digital photography and low magnification microscopy using a Keyence VHX-6000. Cross-sectioning of gas gun specimens was accomplished using a band saw.

Table 1: Architectures designed for Charpy v-notch evaluation.

| Architect. Number | Specimen Orientation | Layer thickness (mm) | Onyx Infill | Kevlar reinforcement |
|--------------------------|-----------------------------|-----------------------------|--------------------|--|
| 1 | XY notch down | 0.100 | TRI | No |
| 2 | XY notch side | 0.100 | TRI | No |
| 3 | Z | 0.100 | TRI | No |
| 4 | Z | 0.200 | TRI | No |
| 5 | XY notch down | 0.125 | TRI | No |
| 6 | XY notch down | 0.200 | TRI | No |
| 7 | XY notch side | 0.200 | TRI | No |
| 8 | XY notch down | 0.100 | TRI | ISO (0.27 cu.cm, front & rear) |
| 9 | XY notch side | 0.100 | TRI | ISO (0.26 cu.cm, top & bottom) |
| 10 | Z | 0.100 | TRI | ISO (0.04 cu.cm, both ends) |
| 11 | XY notch down | 0.100 | TRI | CON (0.17 cu.cm, front and rear) |
| 12 | Z | 0.100 | RECT | CON (0.04 cu.cm, both ends) |
| 13 | Z | 0.100 | RECT | ISO (0.04 cu.cm, both ends) |
| 14 | XY notch side | 0.100 | RECT | ISO (0.26 cu.cm, top & bottom) |
| 15 | XY notch down | 0.100 | RECT | ISO, 1.49 cu.cm, full interior of kevlar |
| 16 | XY notch down | 0.100 | RECT | No |
| 17 | XY notch down | 0.100 | RECT | No |
| 18 | XY notch down | 0.100 | HEX | ISO & CON, 0.68 cu.cm, 1 mm at back and at notch |
| 19 | XY notch down | 0.100 | HEX | ISO & CON, 0.72 cu.cm, dual mid center |
| 20 | XY notch down | 0.100 | HEX | ISO & CON, 0.33 cu.cm, single 1mm layer back |
| 21 | XY notch down | 0.100 | HEX | ISO & CON, 0.33 cu.cm, single 1mm layer at notch |
| 22 | XY notch down | 0.100 | HEX | ISO & CON, 0.69 cu.cm, dual (2 x 1mm) at notch |
| 23 | XY notch down | 0.100 | HEX | ISO & CON, 0.69 cu.cm, dual (2 x 1mm) back |
| 24 | XY notch down | 0.100 | RECT | CON, 1.49 cu.cm, filled minus front |

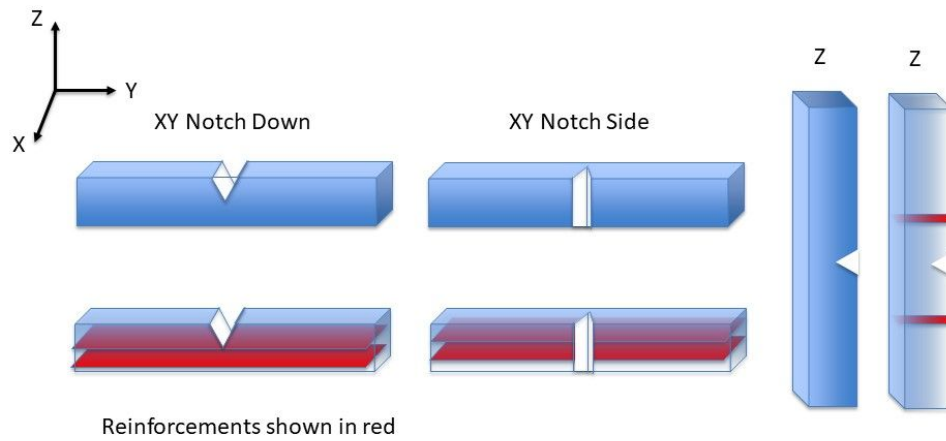


Figure 4: Charpy specimen orientations



Figure 4: REL gas gun used in the experimental study.

3. Results and discussion

3.1 Charpy Impact Tests

The results of the Charpy Impact tests are shown in Table 2 along with the mass and cost for each architectures. All cases had 3 to 4 replicates.

Comparing the impact performance between the XY Notch Down and Z orientation samples (for reference see figure 4), it was observed that the Z orientation is noticeably weaker regardless of the Onyx infill pattern type examined (TRI or RECT). For instance, the reduction in impact strength from Specimen #6 to a similar triangular infill but Z orientation Architecture #4 is 42%. The reduction in impact strength from Architecture #16 (XY notch down) to a similar rectangular infill based on Z orientation such as Architecture #13 is 62%. Here, the comparison between a non-Kevlar reinforced specimen (sample #16) and a Kevlar reinforced Z specimen (sample #13) is valid because the Kevlar is a non-factor in Z orientation, as will later be discussed. The best performing architectures in the Z orientation were the rectangular Onyx infill. For example, compare sample #10 (TRI) against specimen #13 (RECT).

For the effect of layer thickness, XY Notch Side (a.k.a. “flat” in [14]) did not see a significant difference in impact strength between layer thickness of 0.100 mm and 0.200 mm (compare Architecture #2 and #7). This observation differs from that of Caminero et al that showed an increase in impact strength for XY Notch Side as layer thickness increased. For XY Notch Down (or “On-Edge” in [14]), the impact strength of 0.200 mm is greater than that of 0.100 mm and that of 0.125 mm. This appears to contract findings reported by Caminero et al for XY Notch Down (or “On-Edge”). This difference may be the result of the Onyx being more brittle than nylon, a performance associated with the presence of the chopped fiber reinforcement within Onyx.

Unsurprisingly, Kevlar provides no useful role on the impact performance of samples containing the notch parallel to the Kevlar planes; as is the case of the reinforced Z orientation specimens (refer to architecture #3 and #10). However, when the Kevlar reinforcement layer was perpendicular to the notch plane as would be the case in the XY Notch Down orientation, then more energy was required to fracture the specimen. This is observed on architecture #1, which does not contain Kevlar, and sample #8, which has the same architecture but contains 0.27 cm³ of Kevlar in front of the notch and at the rear of the notch. Here, there was an increase of 47% of the energy required for fracture the specimen with the addition of Kevlar. There was an even more dramatic difference when comparing architecture #16 to #15. In this case, by adding a monolithic layer of 1.49 cm³ of Kevlar to the architecture of architecture #15, the impact energy

increased from 0.832 lb ft to 8.394 lb ft. Indeed, the reinforcement being parallel to the XY plane, requires the crack to penetrate the entire layer. In practice, as shown in Figure 6, the fracture path becomes exceptionally tortuous as the crack attempts to progress by delaminating the reinforcement layer away from the Onyx, and tearing the fibers when possible. It should also be noted that the non Kevlar reinforced rectangular Onyx infill specimen (#16) outperformed the non Kevlar reinforced triangular specimen (#1). The rectangular infill pattern has a higher fill setting while the triangular has a narrower infill band.

In the case of the XY Notch Side orientation, the addition of Kevlar slightly increases the impact energy of the samples. Comparing architecture #2 which does not contain Kevlar to #9 which has the same architecture but with 0.26cm³ of Kevlar at the top and bottom of the specimen, it was seen that the presence of the reinforcement increased the impact energy of the printed system by 11%. In the XY Notch Side orientation, only the edge of the reinforcement layer is presented to the crack and tearing and bypassing of the Kevlar is easier at this orientation.

While the highest performance was achieved by Kevlar reinforced specimens with RECT Onyx infill, both cost and machine time are high for such a combination. A good mix of cost, weight, and performance was obtained by HEX Onyx infill patterns with combined ISO and CON reinforcement fill patterns (see architectures #18 to #23).

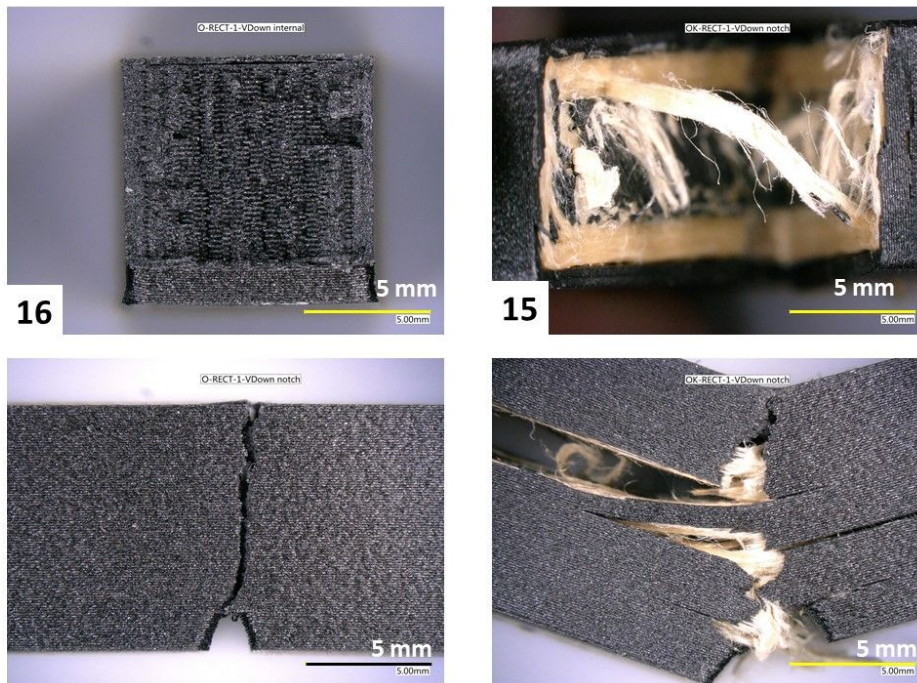


Figure 6: Images of specimens of architecture 15 which is reinforced, versus unreinforced architecture 16. The micrographs show distinctive differences in their fracture behavior, due to presence of the Kevlar fibers.

Table 2: Measured Charpy Impact energy along with calculated mass and cost from Eiger software

| <u>Specimen Name</u> | <u>Average Energy (lb ft)</u> | <u>Total Mass (g)</u> | <u>Cost</u> |
|----------------------|-------------------------------|-----------------------|-------------|
| 1 | 0.624 | 4.72 | \$0.94 |
| 2 | 0.713 | 4.72 | \$0.95 |
| 3 | 0.280 | 4.8 | \$0.96 |
| 4 | 0.446 | 4.71 | \$0.94 |
| 5 | 0.471 | 4.66 | \$0.93 |
| 6 | 0.764 | 4.66 | \$0.93 |
| 7 | 0.726 | 4.66 | \$0.93 |
| 8 | 0.918 | 5.83 | \$1.63 |
| 9 | 0.790 | 5.84 | \$1.62 |
| 10 | 0.254 | 10.57 | \$2.18 |
| 11 | 1.407 | 5.77 | \$1.45 |
| 12 | 0.434 | 12.59 | \$2.58 |
| 13 | 0.319 | 12.59 | \$2.58 |
| 14 | 0.990 | 7.8 | \$2.01 |
| 15 | 8.394 | 7.58 | \$5.69 |
| 16 | 0.833 | 7.01 | \$1.40 |
| 17 | 3.482 | 7.01 | \$1.40 |
| 18 | 3.569 | 6.51 | \$2.49 |
| 19 | 3.153 | 6.36 | \$2.52 |
| 20 | 1.500 | 6.16 | \$1.81 |
| 21 | 2.789 | 6.16 | \$1.81 |
| 22 | 3.786 | 6.34 | \$2.46 |
| 23 | 2.134 | 6.35 | \$2.46 |
| 24 | 4.000 | 6.51 | \$2.49 |

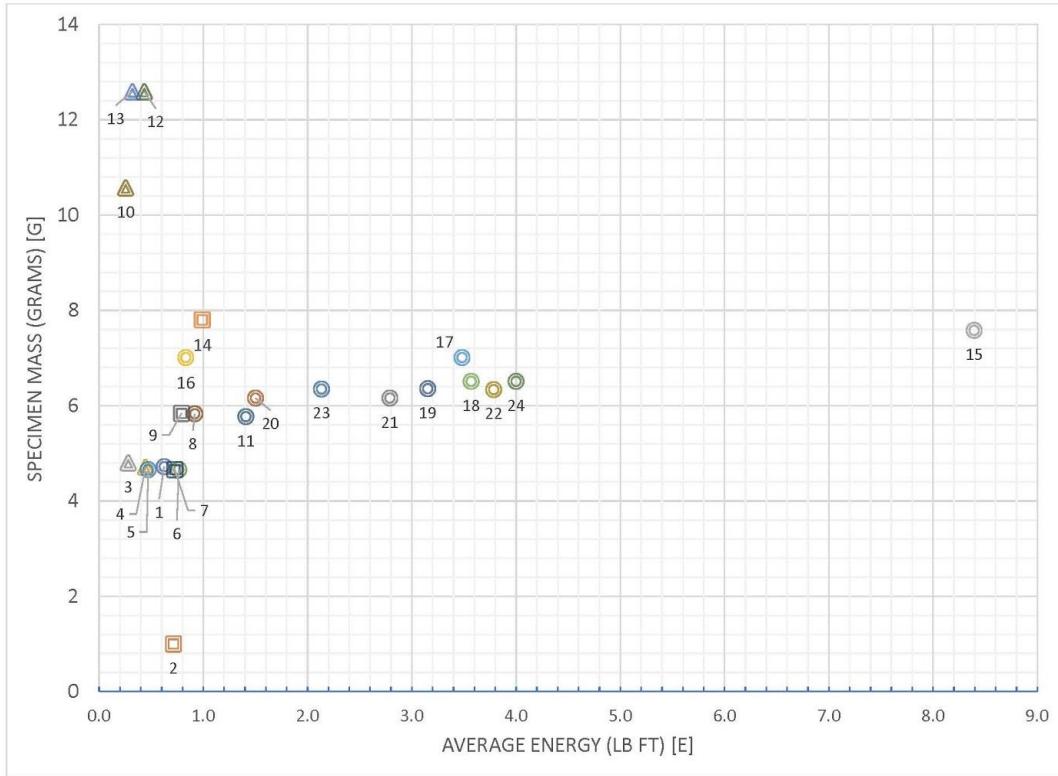


Figure 7: Mass-impact energy relationship of the composites printed by a MarkForged system.

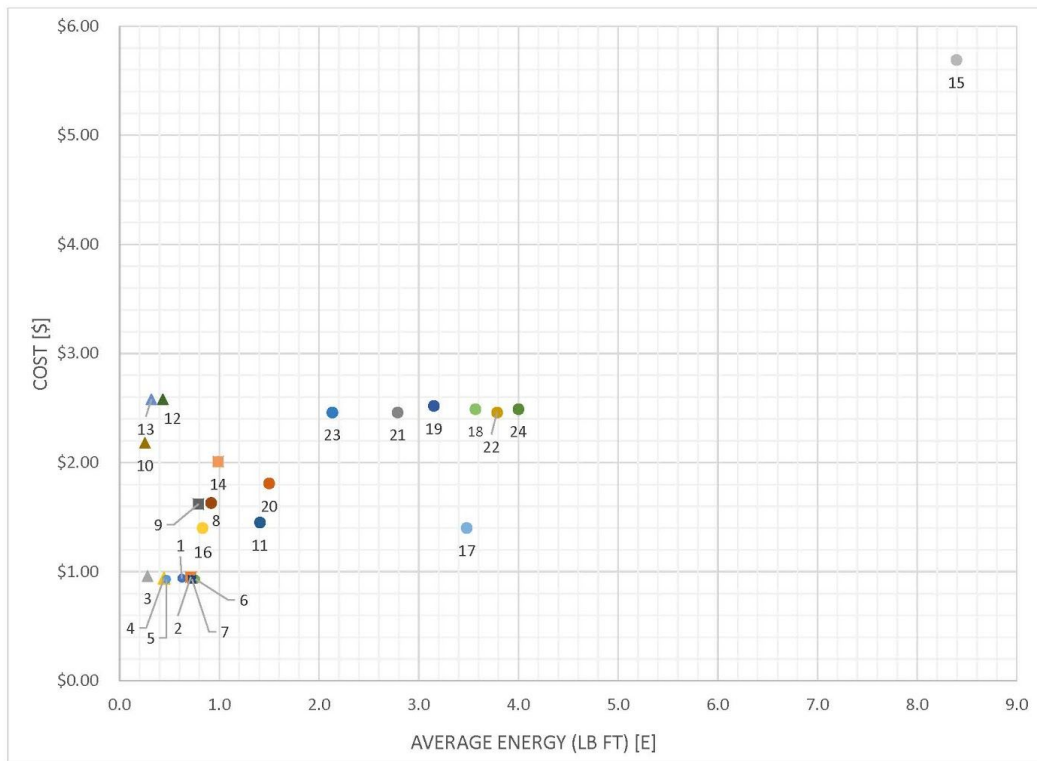


Figure 8: Specimen material cost is plotted against average impact energy

The Charpy test results were here used as an architectural design guidance for the gas gun testing. Figure 7 shows a plot of the average impact energy versus mass, while Figure 8 is a plot of the average impact energy versus cost. The addition of Kevlar is necessary. Higher loadings of Kevlar greatly improved performance but architecture must be taken into account. Architecture #20 had a 1 mm layer of Kevlar at the back side of the specimen away from the notch while #23 doubled the layer at the back side of the specimen. Neither did well but that is likely a function of the Charpy geometry -- by the time the crack reached the back end the specimen would have dramatically folded over. This might not be as relevant in the gas gun test, so it should be tested. But it does indicate architecture matters. Rectangular infill with high density provided high average impact energies but also additional costs.

3.2 Gas gun tests

Four architectures were designed based on the results of the Charpy impact tests. These are shown in Table 3. Architecture G1 had no reinforcement. G2 had reinforcement at one face of the plate. G2 and G3 had nearly the same percent volume of Kevlar reinforcement (36% and 37%) but the Kevlar was placed at two different locations in the samples. Adding reinforcement increases build time due to the physical motion of a second extruder head and the differences in deposition speeds. Kevlar is also much more expensive than Onyx, so the price is greater.

All of the samples here were 6 mm thick plates and all gas gun tests performed were an overmatch. In other words, the projectile completely penetrated the plate for each test. Even reducing the velocity from around 255 m/s to 210 m/s (by reducing the gas pressure from 100 psi to 50 psi) still produced an overmatch on a reinforced plate. Many more tests and plates would have been required to determine a V50 velocity for each architecture at this thickness. However, based on the fracture mechanisms shown by the perforated samples, a performance impact evaluation was here performed. The results are summarized in Table 4.

For the G1 plate architecture, two plates were printed and tested at 255 and 208 m/s. As previously mentioned, both tests completely penetrated the plate as shown in Figure 9. From the sample tested at 255 m/s, it is observed that the back face (opposite of the impact site) shows a damage zone of nearly 14 mm of diameter, with a distinctive X-shaped delamination form. One delamination petal was torn away from the target during projectile exit revealing the triangular infill pattern below it. The X shape of the delamination is likely due to the orientation and rotation of the raster pattern in the face sheets of the build during the building process.

Table 3: Architectures for gas gun testing

| Architect. Number | Layer thickness (mm) | Onyx Infill | Kevlar reinforcement | % Vol Kevlar | Material Cost | Estimated Print Time |
|-------------------|----------------------|-------------|---|--------------|---------------|----------------------|
| G1 | 0.100 | TRI | No | 0 | \$9.53 | 5 h 38 m |
| G2 | 0.100 | TRI | 5 mm Onyx followed by 0.5 mm Kevlar then 0.5 mm Onyx | 8.44 | \$17.3 | 6 h 55 m |
| G3 | 0.100 | HEX | 0.5 mm Onyx on bottom followed by 1 mm of Kevlar, 3 mm of Onyx, 1 mm of Kevlar, 0.5 mm of onyx on top | 35.94 | \$45.74 | 10 h 11m |
| G4 | 0.100 | HEX | 2 mm thick Kevlar ISO and CON reinforcement at center | 37.06 | \$47.63 | 13h 2m |

Table 4: Summary of gas gun results

| Architect. Number | Shot # | Measured Plate Mass (g) | Pressure (psi) | Round velocity (m/s) | Result (CP=complete penetration) |
|-------------------|--|--|--------------------------|--|---|
| G1 | #1 (Plate 1) #2 (Plate 2) | Plate 1: 42.84 Plate 2: 42.92 | 100 50 | 255.0 208.4 | CP, small X-shaped exit delamination CP, large X-shaped exit delamination |
| G2 | #1 (Plate 1) #2 (Plate 1) #3 (Plate 1) #4 (Plate 2) | Plate 1: 46.77 Plate 2: 46.85 | 100 100 100 100 | No Data No Data No Data No Data | For Shots #1-3 CP, small hexagonal shaped delamination and complete removal of the petals. Shot #4: CP, small X-shaped exit delamination |
| G3 | #1 #2 | 57.14 | 100 100 | 256.5 264.4 | CP, left side of target, large X-shaped exit delamination CP, center of target, large X-shaped exit delamination, large X-shaped entrance delamination |
| G4 | #1 | 58.69 | 100 | 257.6 | CP, large X-shaped exit delamination, bulge around entrance |

For the lower velocity (208 m/s) impact, the X-shaped delamination zone was nearly 30 mm a side. This exit damage zone is nearly 5X times that of the zone in the 255 m/s test. This suggests that if the velocity is high enough, the projectile will pass through the target with minimal resistance leaving a small exit hole. At lower velocities such as 208 m/s, the printed

samples would be able to catch the projectile. Here, the structure will “bulge”, leaving a zone of major plastic deformation around the exit hole.

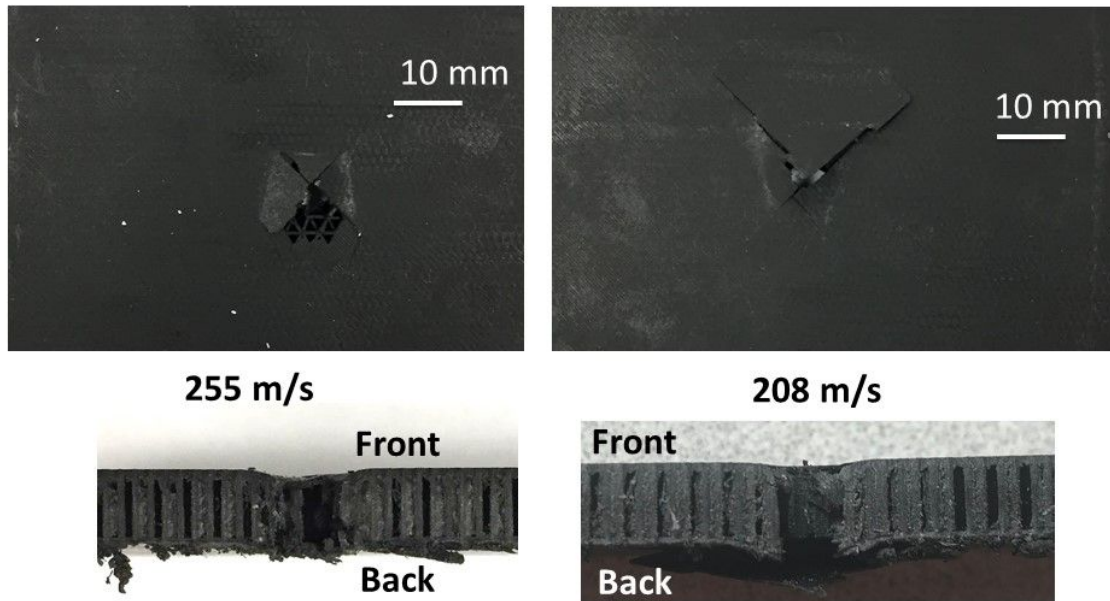


Figure 9: G1 Plate 1 at left and G1 Plate 2 at right

The G2 architecture was reinforced only on one side of the specimen. Here, depending on how the plate was oriented with respect to the incoming projectile, the Kevlar might be closer or further from the impact point. This configuration was tested at 100 psi, which represents a velocity close to 250 m/s; however, error in the chronograph prevented the capture of the impact velocity, and consequently the impact energy.

G2 Plate 1 was shot three times in the orientation with the reinforcement at the front face. Plate 1 is shown in Figure 10. Two shots were relatively close to each other such that the exit damage zones overlapped. Figure 11 is a photograph of a cross section of the damage zone of the two neighboring impacts while Figure 12 is a higher magnification image of one of the holes taken from the microscope. There is considerable ductile plastic deformation of the Kevlar fiber layers. Followed by a conical damage zone of spall that delaminates the back wall of the target plate. The back wall is completely separated from the target (evident on all exit holes in Figure 10) but the damage zone is relatively small meaning that this architecture is highly overmatched.

Figure 13 is a microscope image of the stand-alone hole in G2 Plate 1. It should be noted that entry hole is smaller than the projectile diameter. This indicates that there was expansion to allow the projectile to pass and followed by elastic contraction. It is elucidated, that the

triangular infill has a degree of compliance that accommodates the projectile while passing through the sample. The exit zone shape is characteristic of all of the G2 Plate 1 impact sites in that it is hexagonal. This is likely due to the triangular infill.



Figure 10: G2 Plate 1 front face at left and back face at right.



Figure 11: G2 Plate 1 cross section

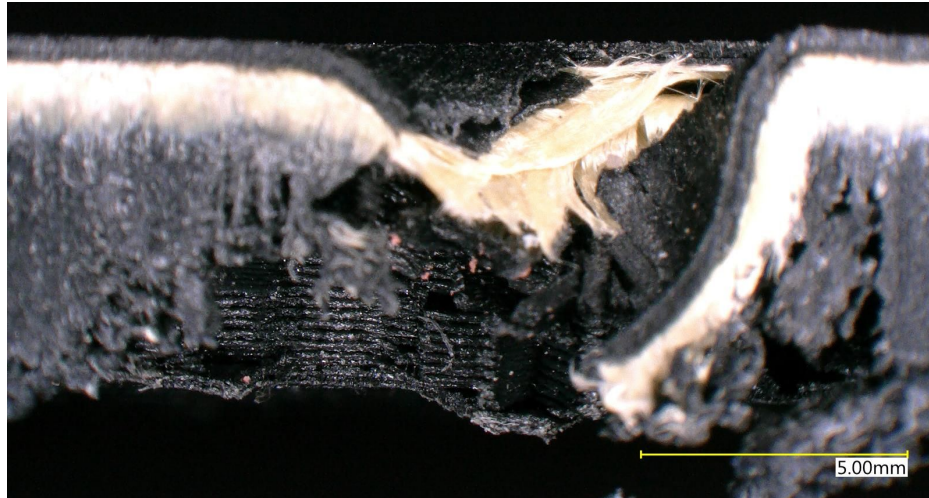


Figure 12: Close up image of the right hole seen in Figure 11.

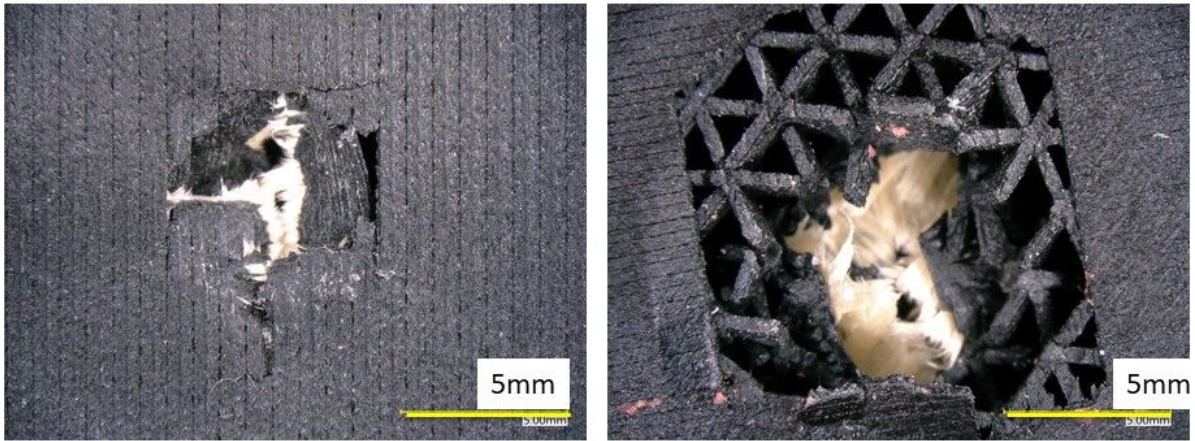


Figure 13: Impacted G2 Plate 1 based on a triangular infill. Entry hole (left), and exit zone (right).

The impacted G2 Plate 2 with the Kevlar placed in the back of plate is shown in Figure 14. At the exit damage zone, the back face wall is delaminated but not torn away. There is more containment than that observed in Plate 1, but the architecture is still highly overmatched as evidenced by the small size of the exit zone. Figure 15 shows the cross section of the G2 plate 2. In this figure, it is shown that the spall region is narrower and more cylindrical than the displayed in plate 1. Here, a clear Kevlar delamination layer extending well beyond the exit hole is observed, but no spall cone was observed.

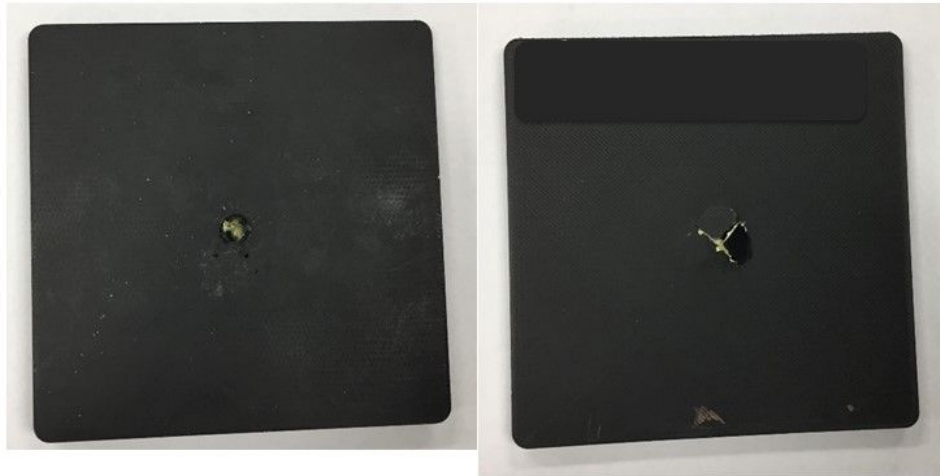


Figure 14: Impacted G2 Plate 2. Front face (left) and back face (right).

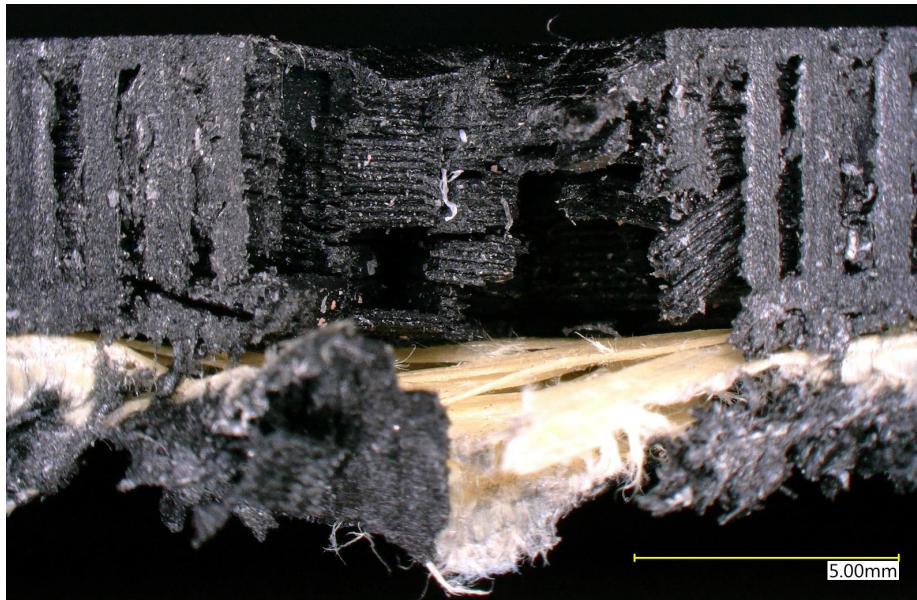


Figure 15: Micrograph of G2 Plate 2. The front face is on the top of the sample.

For architecture G3, the reinforcement was symmetric so orientation was not an issue. Two shots were fired. The first was left of the target center due to debris in the sabot catching system resulting in a skewed shot. However, there was a large half X shaped delamination (the half X due to the proximity to the target edge which was fixed). This offered an opportunity for a second shot which did impact the center. The G3 target plate is shown in Figure 16. Interestingly, a massive delamination zone appeared at the *entry* point as well as at the exit point. The large exit damage zones infers that this architecture is has a superior impact performance compared to G1 and G2 due to the impact energy being dissipated in large delamination areas. If the plate thickness can be increased while maintaining the percent volume infill, this architecture

would stop the projectile at this velocity. The large entry site delamination is possibly the result of a shockwave deflection along the front face or due to a spring-back effect from the near-surface Kevlar layer after the projectile has passed. There may have also been an accumulation of damage from the first shot.

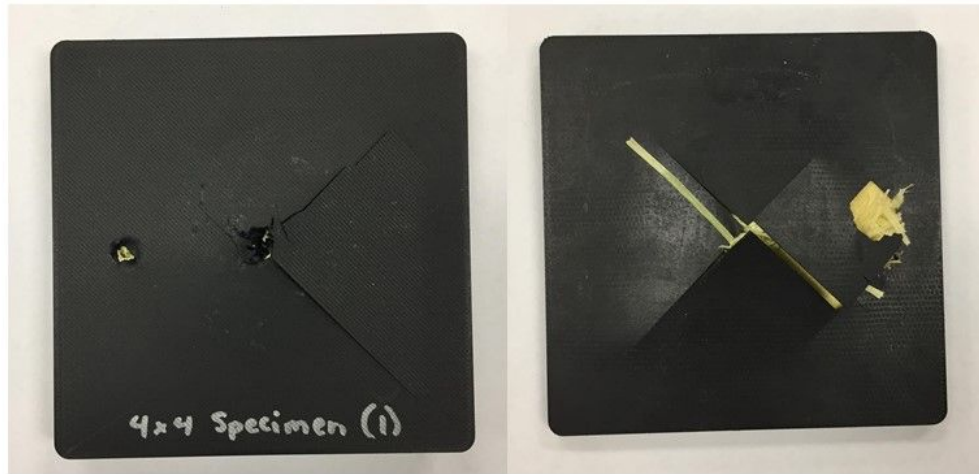


Figure 16: Impacted G3 target plate. Front face (left), and back face (right).

Figure 17 is a cross sectional view of the G3 target plate. Both impact sites are shown. There is significant plastic deformation of the Kevlar layer and the Onyx layer sandwiched between. Each Kevlar layer in this architecture is twice as thick as the Kevlar in G2. A high magnification image of the center hole is shown in Figure 18.



Figure 17: A cross section of the G3 target plate through both impact locations



Figure 18: Image of the center hole (Shot #2) on the G3 sample. The blue part in the image is a fragment of the sabot.

The G4 system was also investigated. Here, the G4 has the same thickness of Kevlar as G3, but all the reinforcement is contained in the middle of the plate. Post-impact images of the target plate can be seen in Figure 19. The figure shows that the projectile produced a large exit damage zone on this plate, indicating that this plate may be near being able to stop the projectile. The cross section of the G4 specimen is shown in Figure 20 where plastic deformation of the Kevlar is clearly seen. The figure also shows delamination at the interface between the Kevlar and the Onyx, an effective mechanism for dissipating energy. This is a thicker delamination than seen in the other architectures. A higher magnification image of the penetration location is shown in Figure 2, where it is observed an intralaminar delamination within the Kevlar fiber. Here, the hole is narrow and no spall cone were displayed.

Further optical analysis was carried out on the impacted zone from the top view with a Keyence microscope using 2D and 3D capabilities (see figure 21). Figure 21 shows a delamination bulge at the entry hole, a feature attributed to a shockwave deflection from Kevlar layer.

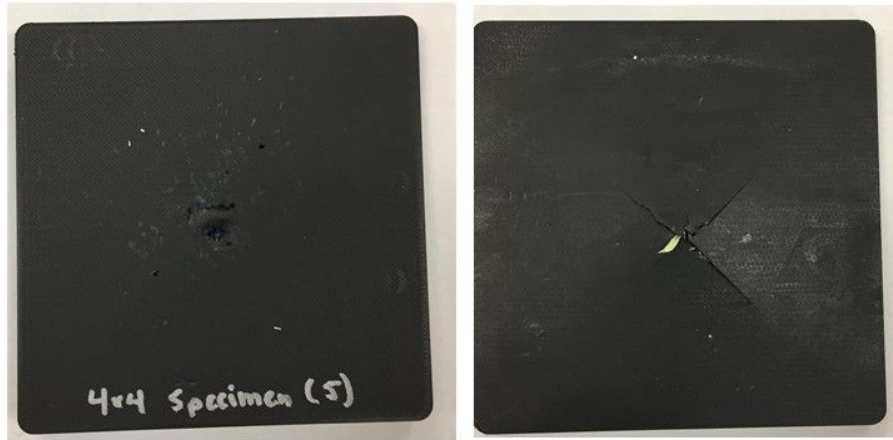


Figure 19: Impacted G4 target plate. Front face (left), and back face (right).

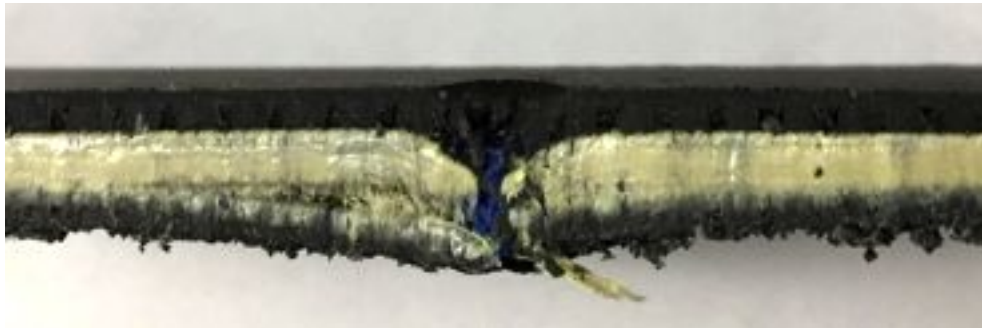


Figure 20: A cross section of the impacted G4 target plate.

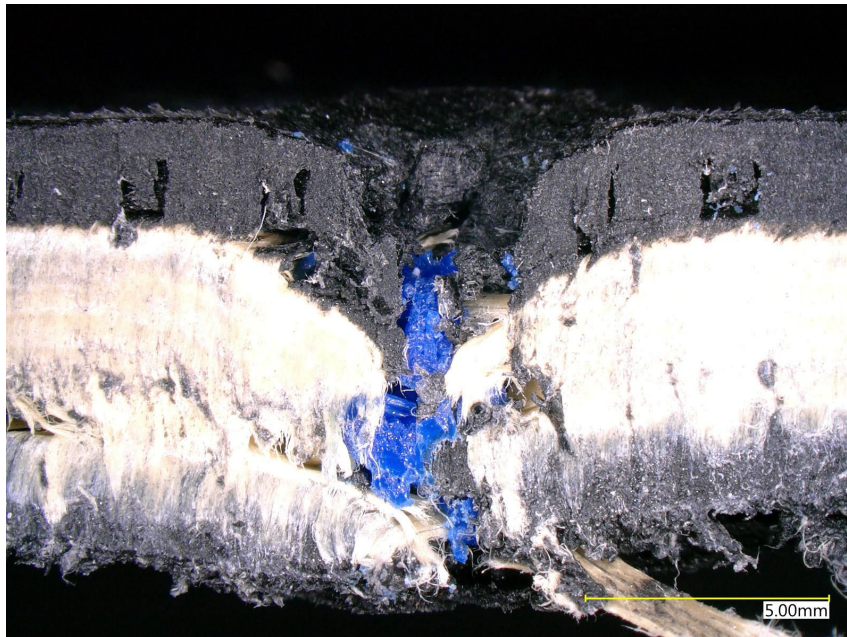


Figure 21: A microscope image of the penetration zone in the G4 target plate. The blue fragments are from the sabot.

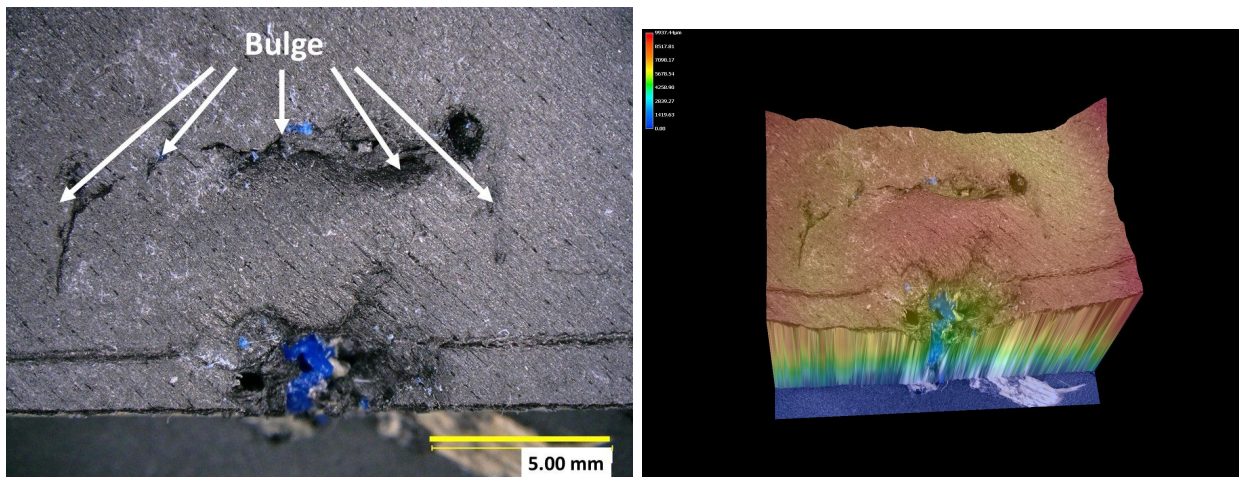


Figure 21: A microscope image of the penetration zone in the G4 target plate from the top view (left). The blue fragments are from the sabot. 3D rendering at right.

4. Conclusions

The following conclusions can be made from the Charpy impact testing:

- The Z orientation is noticeably weaker than the XY Notch Down orientation regardless of Onyx infill pattern type examined.
- The XY Notch Side orientation did not see a significant difference in impact strength between layer thickness of 0.100 mm and 0.200 mm. For XY Notch Down, the impact strength of 0.200 mm is greater than that of 0.100 mm and 0.125 mm. The difference in findings from previous research [14] may be the result may be the result of the Onyx being more brittle than nylon, a performance associated with the presence of the chopped fiber reinforcement within Onyx.
- Kevlar reinforcement provides no useful role if the impact notch is parallel to the Kevlar reinforcement planes as in the case in the reinforced Z orientation specimens.
- In the XY Notch Down orientation, the Kevlar reinforcement layer is perpendicular to the notch plane then more energy is required to fracture the specimen. (see architecture #16 with a layer of 1.49 cu.cm of Kevlar versus architecture #15, the impact energy leaped from 0.832 lb ft to 8.394 lb ft!). The fracture path becomes exceptionally tortuous as the crack will attempt to progress by delaminating the reinforcement layer away from the Onyx and tearing fiber when possible. This is similar to observations from previous research involving nylon (not Onyx) reinforced by Kevlar [14].
- In the case of the XY Notch Side orientation, the addition of Kevlar is of some value but not dramatic. In the XY Notch Side orientation, only the edge of the reinforcement layer is presented to the crack and tearing and bypassing of the Kevlar is easier at this

orientation. This also agrees with observations from previous research involving nylon reinforced by Kevlar [14].

- While the highest performance was achieved by Kevlar reinforced specimens with rectangular Onyx infill, both cost and machine time are high for such a combination. A desirable mix of cost, weight, and performance was obtained by HEX Onyx infill patterns with combined ISO and CON reinforcement fill patterns).

The following conclusions can be made from the gas gun projectile impact testing:

- From the difference in velocity testing, the exit damage zone will be small when overmatch is high. The exit damage zone will be large when overmatch is small which means the architecture is close to stopping the projectile at that target thickness and projectile velocity. Based on this observation, G1 and G2 architectures were highly overmatched. G3 and G4 architectures were less overmatched. Increasing the plate thickness to 8 mm or 10 mm and while keeping the relative % percentage and location of reinforcement should result in the projectile being stopped at approximately 255 m/s.
- For a sparse infill, the entry hole of the round will be less than the diameter of the impact projectile as the structure will elastically expand and then contract. However, the exit zone will be larger due to plastic deformation and spall. There will be an exit damage zone where the surface layer on the back side of the target will delaminate and even tear off.
- Architecture is important. If the Kevlar is positioned near the surface of the front or impact side of the target and there is no reinforcement near the exit or back side of the target, there will be a spall cone. If there is reinforcement near the back side of the target, the spall cone is eliminated.
- Surface delamination appears to follow raster patterns and form an X shape. The depth of delamination can be a function of the depth of the Kevlar layer. In architecture G3 the Onyx delamination layer extended 0.5 mm deep to the Kevlar layer. Architecture G4 had a thicker delamination layer that extended to the Kevlar layer which was 2 mm deep.

Another general conclusion is that Charpy V-notch testing is an imperfect predictor of gas gun performance. The Charpy geometry has a notch that extends across the width of the specimen. The gas gun impact is localized. What works well in Charpy might not work well in gas gun impact. For Charpy specimens, reinforcement needs to be close to the notch in order to increase impact energy. For gas gun targets, the reinforcement should be away from the impact site in order to prevent the formation of a spall cone. Regardless of method, a key finding is that architecture determines the performance against impact.

References

1. Yang B. Blade containment evaluation of civil aircraft engines. *Chin J Aeronaut.* 2013;26: 9–16.
2. Kim H, DeFrancisci G, Chen ZM, Rhymer J. Impact damage formation on composite aircraft structures. UCSD FAA JAMS Paper, Technical Review Meeting. 2012. Available: https://www.niar.wichita.edu/niarworkshops/Portals/0/UCSD_Kim_PP.pdf
3. Richardson WJ, West T. Serious birdstrike accidents to military aircraft: updated list and summary. Proceedings of 25th International Bird Strike Committee Meeting Amsterdam, Netherlands. 2000. pp. 67–98.
4. Georgiadis S, Gunnion AJ, Thomson RS, Cartwright BK. Bird-strike simulation for certification of the Boeing 787 composite moveable trailing edge. *Compos Struct.* 2008;86: 258–268.
5. Christiansen E, Lear D. Micrometeoroid and Orbital Debris Environment and Hypervelocity Shields. 2012; Available: <https://ntrs.nasa.gov/archive/nasa/casi.ntrs.nasa.gov/20120002584.pdf>
6. David NV, -L. Gao X, Zheng JQ. Ballistic Resistant Body Armor: Contemporary and Prospective Materials and Related Protection Mechanisms. *Appl Mech Rev. American Society of Mechanical Engineers;* 2009;62: 050802.
7. McCauley JW, Crowson A, Gooch WA Jr, Rajendran AM, Bless SJ, Logan K, et al. *Ceramic Armor Materials by Design.* John Wiley & Sons; 2012.
8. Conner BP, Manogharan GP, Martof AN, Rodomsky LM, Rodomsky CM, Jordan DC, et al. Making sense of 3-D printing: Creating a map of additive manufacturing products and services. *Additive Manufacturing.* 2014;1–4: 64–76.
9. Rioja RJ, Conner BP, Kamat RG. Crashworthy structures formed of multilayered metallic materials [Internet]. US Patent. 9067623, 2015. Available: <https://patentimages.storage.googleapis.com/bb/3c/1e/a79baf7d0d506e/US9067623.pdf>
10. Sinke J. Development of fibre metal laminates: concurrent multi-scale modeling and testing. *J Mater Sci.* Springer; 2006; Available: https://idp.springer.com/authorize/casa?redirect_uri=https://link.springer.com/article/10.1007/s10853-006-0206-5&casa_token=x7ul9rZAePcAAAAA:jL8BmRSczu3xhk9AkWZr2ZMawrLJXsVZdbY_d-POWlyQYsGp356lp8yXgITvNtHLIljehp3ekJm6kFI
11. Moxson VS, Ivanov E. Bulletproof lightweight metal matrix macrocomposites with controlled structure and manufacture the same [Internet]. US Patent. 6635357, 2003. Available:

<https://patentimages.storage.googleapis.com/cf/bc/cb/31d474fb655d93/US6635357.pdf>

12. Our materials. In: Markforged [Internet]. [cited 12 Aug 2018]. Available: <https://markforged.com/materials/>
13. Melenka GW, Cheung BKO, Schofield JS, Dawson MR, Carey JP. Evaluation and prediction of the tensile properties of continuous fiber-reinforced 3D printed structures. *Compos Struct.* 2016;153: 866–875.
14. Caminero MA, Chacón JM, García-Moreno I, Rodríguez GP. Impact damage resistance of 3D printed continuous fibre reinforced thermoplastic composites using fused deposition modelling. *Composites Part B.* 2018;148: 93–103.